



**HAL**  
open science

# Ground subsidence effects on simulating dynamic high latitude surface inundation under permafrost thaw using CLM5

Altug Ekici, Hanna Lee, David S Lawrence, Sean Swenson, Catherine Prigent

## ► To cite this version:

Altug Ekici, Hanna Lee, David S Lawrence, Sean Swenson, Catherine Prigent. Ground subsidence effects on simulating dynamic high latitude surface inundation under permafrost thaw using CLM5. Geoscientific Model Development Discussions, 2019, pp.1-15. 10.5194/gmd-2019-4 . hal-02389468

**HAL Id: hal-02389468**

**<https://hal.science/hal-02389468>**

Submitted on 29 May 2024

**HAL** is a multi-disciplinary open access archive for the deposit and dissemination of scientific research documents, whether they are published or not. The documents may come from teaching and research institutions in France or abroad, or from public or private research centers.

L'archive ouverte pluridisciplinaire **HAL**, est destinée au dépôt et à la diffusion de documents scientifiques de niveau recherche, publiés ou non, émanant des établissements d'enseignement et de recherche français ou étrangers, des laboratoires publics ou privés.



Distributed under a Creative Commons Attribution 4.0 International License



1 **Ground subsidence effects on simulating dynamic high latitude**  
2 **surface inundation under permafrost thaw using CLM5**

3  
4 **Altug Ekici<sup>1,2,3</sup>, Hanna Lee<sup>1</sup>, David M Lawrence<sup>4</sup>, Sean C Swenson<sup>4</sup>, and Catherine**  
5 **Prigent<sup>5</sup>**

6  
7 <sup>1</sup>NORCE Norwegian Research Centre, Bjerknes Centre for Climate Research, Bergen, Norway

8 <sup>2</sup>Climate and Environmental Physics, Physics Institute, University of Bern, Bern, Switzerland

9 <sup>3</sup>Oeschger Centre for Climate Change Research, University of Bern, Bern, Switzerland

10 <sup>4</sup>Climate and Global Dynamics Division, National Center for Atmospheric Research, Boulder,  
11 Colorado, USA

12 <sup>5</sup>LERMA, Observatoire de Paris, PSL Research University, CNRS, UMR 8112, F-75014, Paris,  
13 France

14  
15 Correspondence to: [ekici@climate.unibe.ch](mailto:ekici@climate.unibe.ch)

16  
17 **Abstract**

18 Simulating surface inundation is particularly challenging for the high latitude  
19 permafrost regions. Ice-rich permafrost thaw can create expanding thermokarst  
20 lakes as well as shrinking large wetlands. Such processes can have major  
21 biogeochemical implications and feedbacks to the climate system by altering the  
22 pathways and rates of permafrost carbon release. However, the processes  
23 associated with it have not yet been properly represented in Earth system  
24 models. We show a new model parameterization that allows direct  
25 representation of surface water dynamics in CLM (Community Land Model), the  
26 land surface model of several Earth System Models. Specifically, we coupled  
27 permafrost-thaw induced ground subsidence and surface microtopography  
28 distribution to represent surface water dynamics in the high latitudes. Our  
29 results show increased surface water fractions around western Siberian plains  
30 and northeastern territories of Canada. Additionally, localized drainage events  
31 correspond well to severe ground subsidence events. Our parameterization is  
32 one of the first steps towards a process-oriented representation of surface  
33 hydrology, which is crucial to assess the biogeochemical feedbacks between land  
34 and the atmosphere under changing climate.

35  
36 **1. Introduction**

37 Northern high latitudes experience pronounced warming due to Arctic  
38 amplification (Serreze and Francis, 2006). Within the last decades, temperature  
39 increase in the Arctic has been twice the amount of that in the tropics (Solomon  
40 et al., 2007). The abrupt increase in Arctic temperatures threatens to destabilize  
41 the global permafrost areas and can alter land surface structures, which can lead  
42 to releasing considerable amounts of permafrost carbon as greenhouse gases to  
43 the climate system (Schuur et al., 2008). The balance between CO<sub>2</sub> and CH<sub>4</sub>  
44 release from permafrost depends largely on the organic matter decomposition  
45 pathway; larger inundated areas release more CH<sub>4</sub> than CO<sub>2</sub> using the anaerobic  
46 pathway but overall release of greenhouse gases is greater under aerobic  
47 conditions (Lee et al. 2014; Treat et al. 2015). The main natural sources of CH<sub>4</sub>  
48 emissions are from tropical wetlands, however the contributions from high  
49 latitude wetlands are increasing each decade (Saunois et al., 2016) with further  
50 thawing of permafrost.

51



1 With high percentage of surface wetland coverage (Grosse et al., 2013; Muster et  
2 al., 2017), characterizing high latitude CH<sub>4</sub> emissions require detailed process  
3 representations in models. However, Earth system models (ESMs) used in the  
4 future climate projections struggle to represent the complex  
5 physical/hydrological changes in the permafrost covered high latitude regions.  
6 Therefore, it is necessary to improve model representation of surface hydrology  
7 processes within the ESMs.

8  
9 Permafrost processes have now been represented commonly within the land  
10 surface models (Lawrence et al., 2008; Gouttevin et al., 2012; Ekici et al., 2014;  
11 Chadburn et al., 2015), however, the complex hydrological feedbacks between  
12 degrading permafrost and thermokarst lake formations have been a major  
13 challenge. An extensive review of wetland modeling activities and an  
14 intercomparison effort of evaluating methane-modeling approaches are given in  
15 Wania et al. (2013) and Melton et al. (2013). These studies, however, do not  
16 include permafrost specific features such as excess ice in frozen soils, therefore  
17 they have tendency to under-represent key processes associated to permafrost  
18 thaw. Excess ice melt within the frozen soils can lead to abrupt changes in the  
19 surface topography, creating subsided ground levels, which can enhance pond  
20 formation often recognized as thermokarst formation. Such changes in surface  
21 microtopography can be very effective in altering the soil thermal and  
22 hydrological conditions (Zona et al., 2011).

23  
24 Lee et al. (2014) implemented surface subsidence processes in the Community  
25 Land Model (CLM: Oleson et al., 2013; Lawrence et al., 2011; Swenson et al.,  
26 2012) to overcome some of the limitations in representing processes associated  
27 with permafrost thaw and subsequent land surface subsidence. The surface  
28 conditions altered by the subsidence events change the microtopography of the  
29 area, which can further modify the surface hydrological conditions in reality. Lee  
30 et al. (2014) did not further couple the land surface subsidence with hydrological  
31 processes to represent subsequent changes in local hydrology created under  
32 permafrost thawing. Here we developed a conceptual coupling of excess ice  
33 melting and subsequent land surface subsidence with hydrology and show how  
34 implementing permafrost thaw induced subsidence affects surface  
35 microtopography distribution and surface inundation in the CLM model.

## 36 37 **2. Methods**

38 Simulating the effects of permafrost thaw on surface water dynamics requires a  
39 complex interaction of thermodynamics and hydrology within the model. Here  
40 we use the 1° spatial resolution simulations of CLM5 (Lawrence et al., submitted  
41 2018) to represent such dynamics. CLM is a complex, process based terrestrial  
42 ecosystem model simulating biogeophysical and biogeochemical processes  
43 within the soil and vegetation level. Lee et al. (2014) have presented the excess  
44 ice implementation into CLM. The ground excess ice data from International  
45 Circum-Arctic Map of Permafrost and Ground-Ice Conditions (Brown et al., 1997)  
46 are used to create an initial soil ice dataset to be prescribed into the model. The  
47 excess ice in the model undergoes physical phase change but most importantly  
48 melting ice allows a first-order estimation of land surface subsidence under  
49 permafrost thaw.



1 In CLM, surface inundated fraction ( $f_{h2osfc}$ ) of each grid cell is calculated by using  
2 the microtopography distribution ( $\sigma_{micro}$ ) and the surface water level ( $d$ ) of the  
3 grid cell (Eq. 1 - 3).  
4

$$f_{h2osfc} = \frac{1}{2} \left( 1 + \operatorname{erf} \left( \frac{d}{\sigma_{micro} \sqrt{2}} \right) \right)$$

5  
6  
7 Eq.1: Parameterization of surface inundated fraction ' $f_{h2osfc}$ ' using an error function of  
8 surface water level ' $d$ ' (height in m relative to the gridcell mean elevation) and  
9 microtopography distribution ' $\sigma_{micro}$ ' (m).  
10

$$\sigma_{micro} = (\beta + \beta_0)^\eta$$

11  
12  
13 Eq. 2: Microtopography distribution ' $\sigma_{micro}$ ' as a function of slope, where  $\beta$  is the  
14 prescribed topographic slope.  
15

$$\beta_0 = (\sigma_{max})^{\frac{1}{\eta}}$$

16  
17  
18 Eq. 3: Adjustable coefficient  $\beta_0$  as a function of maximum topographical distribution  
19 ' $\sigma_{max}$ '. Original value for  $\sigma_{max}$  is 0.4 while  $\eta$  is -3.  
20

21 This parameterization is similar to the TOPMODEL approach (Beven and Kirkby,  
22 1979), where a hypsometric function is used to define the height of standing  
23 water ( $d$ ) within the gridbox by assuming a normal statistical distribution of  
24 ground level microtopography. In this study, the subsidence levels from  
25 permafrost thaw induced excess ice melt are coupled with  $\sigma_{micro}$  in order to  
26 represent the naturally occurring subsided landscapes within the permafrost-  
27 affected areas. With increasing excess ice melt, more subsidence occurs and the  
28 amount of subsidence redefines the surface  $\sigma_{micro}$ , which is inversely related to  
29  $f_{h2osfc}$  (Eq. 1). Therefore, to represent increased  $f_{h2osfc}$ ,  $\sigma_{micro}$  has to be decreased  
30 in value. However,  $\sigma_{micro}$  is the statistical distribution of surface  
31 microtopography, hence cannot be directly related to physical subsidence levels.  
32 Therefore, a preliminary method of relating  $\sigma_{micro}$  to an order of magnitude lower  
33 ground subsidence levels is used (Eq. 4).  
34

$$\sigma'_{micro} = \begin{cases} \sigma_{micro} - s \div b, s < 0.5 \\ \sigma_{micro} + s \div b, s \geq 0.5 \end{cases}$$

35  
36  
37 Eq. 4: New microsigma parameterization ' $\sigma'_{micro}$ ' where ' $s$ ' is the subsidence in meters  
38 and ' $b$ ' is the adjustable parameter set to 10.  
39

40 We implemented a conditional formulation regarding the severity of subsidence.  
41 In general, the surface is forced to allow more ponding of water with moderate  
42 levels of subsidence. However, advance levels of excess ice melt can degrade the  
43 surface levels so much that the small troughs created from the initial degradation  
44 can connect to create a drainage system that the grid box can no longer support



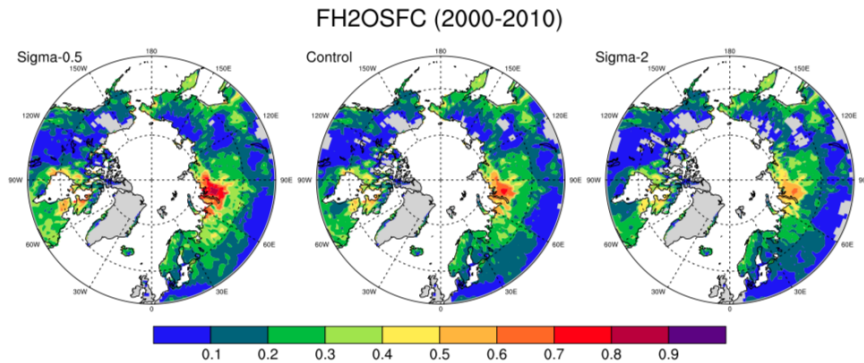
1 any ponding (Liljedahl et al., 2016). For this reason, the excess ice melt has a  
2 reversed effect on  $\sigma_{\text{micro}}$  after a threshold value of 0.5 m (Eq.4). Choice of this  
3 threshold value is discussed in the following section.

4  
5 We performed several experiments using CLM5 to assess the general response of  
6 surface hydrology to changing microsigma parameter values. First, the  
7 dependence of  $f_{\text{h2osfc}}$  to  $\sigma_{\text{micro}}$  is investigated by doubling  $\sigma_{\text{micro}}$  (experiment:  
8 Sigma-2) and reducing it by half (experiment: Sigma-0.5). Afterwards, the new  
9  $\sigma_{\text{micro}}$  parameterization (experiment: Exice) is compared to the default model  
10 version (experiment: Control), where subsidence does not alter  $\sigma_{\text{micro}}$  or  $f_{\text{h2osfc}}$   
11 and to a satellite driven data product (GIEMS, the Global Inundation Extent from  
12 Multiple Satellites, Prigent et al., 2012). All experiments include 155-year  
13 transient simulations following a spin up procedure of repeating 1901-1930  
14 climate forcing for 100 years. The transient 155-year simulation represents the  
15 time period from 1860 till 2015. CRU-NCEP (Viovy, 2009), a combined dataset of  
16 Climate Research Unit (CRU) and National Center for Environmental Protection  
17 (NCEP) reanalysis datasets, is used as the atmospheric forcing for these  
18 experiments.

19  
20 The GIEMS surface inundation dataset from Prigent et al. (2007, 2012) is used to  
21 compare the simulated inundated fractions. GIEMS uses a combination of  
22 satellite observations to derive the distribution and dynamics of the global  
23 surface water extent. The inundated areas are calculated using passive  
24 microwave observations from Special Sensor Microwave/Imager (SSM/I),  
25 active microwave observations from the scatterometer on board the European  
26 Remote Sensing (ERS) satellite and the normalized difference vegetation index  
27 (NDVI) from the Advanced Very High resolution Radiometer (AVHRR). The  
28 dataset provides monthly-mean values of surface water area from 1993 to  
29 2007, with a spatial resolution of 0.25°. The dataset is spatially projected onto a  
30 1° resolution grid for comparison with the model results.

### 31 32 **3. Results and Discussion**

33 In our experiments, surface inundation ( $f_{\text{h2osfc}}$ ) increases where surface  
34 microtopography distribution ( $\sigma_{\text{micro}}$ ) decreases (Fig. 1) as expected from the  
35 CLM parameterization. When  $\sigma_{\text{micro}}$  decreases (Sigma-0.5) compared to the  
36 original value (shown in Supplementary Figure S1), it results in very high  $f_{\text{h2osfc}}$   
37 over western Siberia and Hudson Bay area, while increasing  $\sigma_{\text{micro}}$  (Sigma-2)  
38 results in lower  $f_{\text{h2osfc}}$  in general. In the original CLM parameterization,  $f_{\text{h2osfc}}$  is  
39 calculated with a static microtopography index (Fig. S1) derived from a  
40 prescribed topographic slope dataset (Oleson et al., 2013).



1  
2 Fig. 1: High latitude ( $>50^{\circ}\text{N}$ ) maps of simulated surface water fractions ( $f_{h2osfc}$ ) from  
3 Control, Sigma-0.5, and Sigma-2.0 experiments with different microsigma distributions  
4 averaged for the period 2000-2010.

5  
6 Our results illustrate the dependence of  $f_{h2osfc}$  on  $\sigma_{micro}$  and how certain range of  
7  $\sigma_{micro}$  values can result in very high  $f_{h2osfc}$ . This relation emphasize the need for a  
8 dynamic circum-Arctic  $\sigma_{micro}$  value to capture the natural variability of surface  
9 conditions when representing permafrost thaw associated hydrological changes.  
10 In the Exice experiment, coupling excess ice melt induced ground subsidence to  
11  $\sigma_{micro}$  leads to significant changes in surface hydrology (Fig. 2). In our  
12 simulations,  $\sigma_{micro}$  is consistently lower in Exice compared to Control at the end  
13 of the 20th century (Fig. 2a). This is the model representation of increased  
14 variability in surface microtopography due to uneven subsidence events within  
15 the gridcell. Particularly larger inundated fractions are simulated around  
16 western Siberia and northeast Canada, which conform well to the observational  
17 datasets of peatland distribution (Tarnocai et al., 2007; 2009). Several other  
18 observational estimates agree on the spatial distribution of high latitude  
19 peatlands, where most of the wetland formations are expected in the future  
20 (Melton et al., 2013). Therefore, the new parameterization of surface inundated  
21 fraction is a stepping-stone towards a more realistic representation of surface  
22 hydrology in permafrost-affected areas. Other modeling studies support these  
23 results with similar spatial patterns of surface wetland distributions (Wania et  
24 al., 2013; Melton et al., 2013). In the previous version of CLM, simulated  
25 inundated area shows slightly different patterns (Riley et al., 2011), mainly due  
26 to non-process based description of inundated fractions. We emphasize that  
27 although our parameterization is only conceptual, this is the first attempt  
28 towards coupling permafrost thaw associated land surface subsidence with  
29 hydrological changes in a land surface model within an ESM.

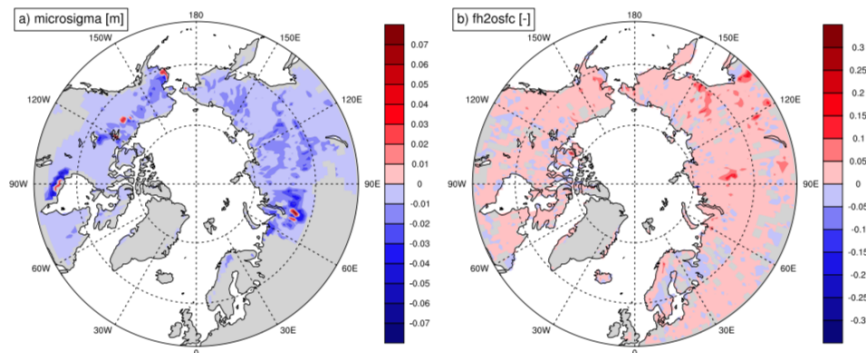
30  
31 By introducing the effects of ground subsidence on  $\sigma_{micro}$ , a dynamic inundated  
32 fraction is calculated. However, there is no observed dataset to evaluate the  
33 relation between subsidence and ground topography, therefore an assumption  
34 had to be made regarding this coupling. In this study, changes in  $\sigma_{micro}$  are  
35 proportional to the changes in ground subsidence with the difference in an order  
36 of magnitude. This assumption is put to test by doubling and halving the initial  
37  $\sigma_{micro}$  values and the results show 10 to 20 % change in surface inundated  
38 fractions (Fig. 1). The difference in dynamic parameterization (Fig. 2b) stays in





1 between these values and on average shows a 10 – 15 % increase, thus  
2 supporting the coupling assumption.

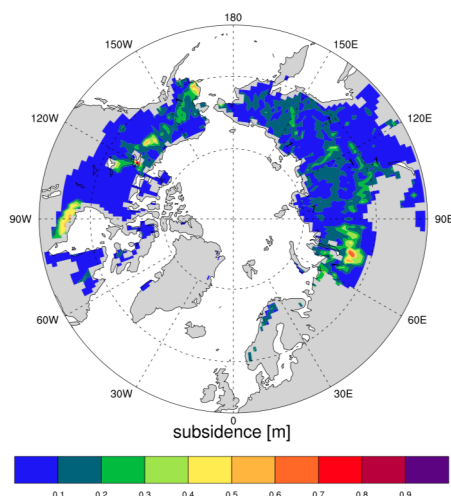
Exice-Control (2000-2010)



3  
4 Fig. 2: Effects of coupled subsidence-microsigma parameterization on ' $\sigma_{\text{micro}}$ ' and ' $f_{\text{h2osfc}}$ '  
5 from  $>50^\circ\text{N}$  difference maps of Exice-Control experiments for the period 2000-2010.  
6

7 As expected, the  $f_{\text{h2osfc}}$  and  $\sigma_{\text{micro}}$  changes are directly related to the ground  
8 subsidence processes in most cases. Exice experiment produces land surface  
9 subsidence in some gridcells (Fig. 3) similar to the spatial patterns exhibited in  
10  $\sigma_{\text{micro}}$  and  $f_{\text{h2osfc}}$  in Fig. 2, suggesting that melting of excess ice directly affects  
11 changes in surface hydrology. This is most pronounced around western Siberia,  
12 south of Hudson Bay and around northwestern Canada and central Alaska,  
13 where initial excess ice was large (Lee et al. 2014). Simulated ground subsidence  
14 is directly associated to changes in surface inundated fraction ( $f_{\text{h2osfc}}$ ) described  
15 in Fig. 2.  
16

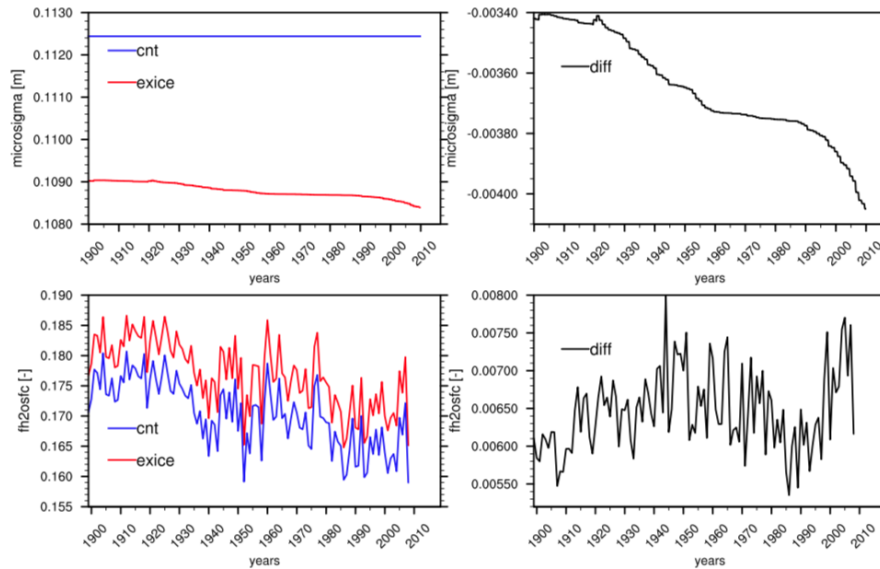
17 As a result of subsidence threshold parameterization (see Methods), reversed  
18 effect of excess ice melting is shown in the  $\sigma_{\text{micro}}$  plots (Fig. 2a), where red points  
19 are directly related to the severe ground subsidence locations (Fig. 3). These  
20 areas consistently exhibit abrupt melting of excess ice leading to increased  $\sigma_{\text{micro}}$ .  
21 Larger negative deviations of  $\sigma_{\text{micro}}$  from the original values were observed in  
22 central Alaska, northwestern Canada, south of Hudson Bay, southwest Russia,  
23 central Siberia, and northern Yakutia regions of Russia (areas with dark blue in  
24 Fig. 2a). In reality, different landscapes should have a different threshold value,  
25 yet our work is aimed to capture the overall changes and general patterns rather  
26 than local conditions, so a preliminary choice of a single threshold value is used.  
27 Same areas show increased  $f_{\text{h2osfc}}$  compared to Control (Fig. 2b). The largest  
28 increases in  $f_{\text{h2osfc}}$  are observed in central Siberia and southeastern Russia, while  
29 some minor decreases in  $f_{\text{h2osfc}}$  values are present in an unevenly distributed  
30 pattern. It is important to add that the choice of 0.5 m threshold is arbitrary and  
31 can be modified according to the surface dataset of excess ice.



1  
2 Fig. 3: High latitude (>50°N) map of ground subsidence simulated from the Exice  
3 experiment averaged for the period 2000-2010.  
4

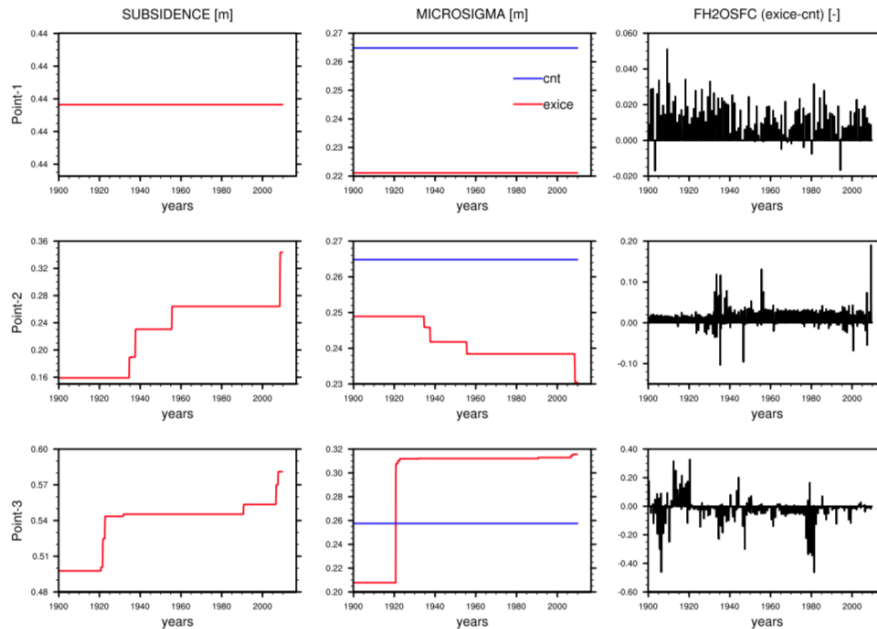
5 Spatially averaged timeseries of  $\sigma_{\text{micro}}$  and  $f_{\text{h2osfc}}$  show that in the Exice  
6 experiment  $\sigma_{\text{micro}}$  decreases over time and  $f_{\text{h2osfc}}$  shows a more dynamic change  
7 during the simulation (Fig. 4). The discrepancy in  $\sigma_{\text{micro}}$  between Exice and  
8 Control in the beginning of the simulation is due to prior excess ice melting  
9 during the spin-up period and the values continue to decrease throughout the  
10 20<sup>th</sup> century, while the decrease halts temporarily during 1960- 1990  
11 (microsigma-diff plot in Fig. 4). Higher  $f_{\text{h2osfc}}$  are observed in Exice experiment,  
12 however, the differences between Exice and Control show a general increase  
13 throughout the simulation except the period between 1960-1990. The spatially  
14 averaged  $f_{\text{h2osfc}}$  values exhibit a non-linear progression during the 20<sup>th</sup> century  
15 (Fig. 4). Mainly the change in climate forcing contributes to this trend. Analyzing  
16 the CRUNCEP atmospheric forcing data suggests that the precipitation pattern  
17 over the experiment domain shows a sudden reduction at the beginning of 1960s  
18 (Fig. S2). Even though the average precipitation starts increasing again, the  
19 lower values contribute to the reduced  $f_{\text{h2osfc}}$  values. Similar changes occur with  
20 the patterns in atmospheric temperatures (Fig. S2), which is a direct forcing for  
21 permafrost thaw and ground subsidence. A process-based representation of  
22  $f_{\text{h2osfc}}$  allows the model to naturally represent the temporal changes in climate.  
23 Hence, our representation of  $f_{\text{h2osfc}}$  will improve the estimation of future surface  
24 hydrological states under changing climatic conditions.





1  
 2 Fig. 4: Timeseries of spatially averaged high latitude ( $>50^{\circ}\text{N}$ )  $\sigma_{\text{micro}}$  and annual  
 3 maximum  $f_{\text{h2osfc}}$  variables from Exice and Control experiments together with the  
 4 timeseries of Exice-Control difference (diff) for the period 1900-2010.

5  
 6 The direct effects of new model parameterization can better analyzed while  
 7 inspecting point scale changes as shown in Fig. 5. The three selected points show  
 8 a range of scenarios to observe the effects of subsidence on microsigma and  
 9  $f_{\text{h2osfc}}$ . Point 1 has no change in subsidence during the simulation and with  
 10 higher microsigma values in Exice (due to prior subsidence in spinup), the  
 11 difference in  $f_{\text{h2osfc}}$  compared to Control simulation is always positive, meaning  
 12 higher surface inundated fractions. In Point 2, Exice microsigma decreases due to  
 13 the increase in subsidence during the simulation. These gradual changes are  
 14 reflected in  $f_{\text{h2osfc}}$ , where sudden increases are shown around 1935 and 1955,  
 15 exactly when the subsidence changes occur. Similarly in Point 3, subsidence  
 16 causes a lower microsigma in the beginning of the simulation; however the  
 17 subsidence values surpass the 0.5m threshold around 1920s, which causes the  
 18 reversed effect on microsigma by increasing it compared to the Control  
 19 experiment. Severe subsidence causing more drainage is represented in this way  
 20 within our parameterization. The  $f_{\text{h2osfc}}$  values show this drainage with a sudden  
 21 decrease at 1920 and continuing with mostly negative values throughout the  
 22 simulation. These scenarios support the validity of our new parameterization  
 23 that can be used for any future climate scenario for a better representation of  
 24 surface hydrology and subsidence coupling.



1  
 2 Fig. 5: Timeseries of subsidence,  $\sigma_{\text{micro}}$ , and  $f_{\text{h2osfc}}$  variables from Exice and Control  
 3 experiments at three selected sites. Point 1: lat 54 N lon 272 E, Point 2: lat 64 N lon 80 E,  
 4 Point 3: lat 65 N lon 70 E.  
 5

6 GIEMS dataset (Prigent et al., 2012) provides the surface area of wetlands for each  
 7 gridbox. Fraction of wetland-covered gridbox is calculated to compare with the model  
 8 results (Fig. 6). The range of estimated surface wetland fraction is different in the  
 9 satellite dataset and model outputs; however, spatial distribution of surface inundated  
 10 area is fairly comparable between the model and the satellite dataset. They both  
 11 exhibit larger inundated fractions in western Siberia and around Hudson Bay. The  
 12 ranges of estimated surface wetland fraction between the satellite dataset and  
 13 model outputs are different due to differences in the definitions of inundated  
 14 areas. However, spatial distribution of surface inundated area is comparable  
 15 between the model and the satellite dataset, where both exhibit larger inundated  
 16 fractions in western Siberia and Hudson Bay. Since our model provides the  
 17 fraction of gridbox that is inundated, the satellite dataset had to be converted  
 18 from actual wetland area to fractions. The GIEMS dataset assumes 773 km<sup>2</sup>  
 19 gridboxes all over the globe (Prigent et al., 2007), which creates grid-size  
 20 problems comparing to model gridbox area. Another issue with such  
 21 comparison stems from the differences in the definition of inundated fraction.  
 22 GIEMS dataset uses satellite observations at different wavelengths to derive the  
 23 wetland area, while the CLM creates the surface inundation with the topography  
 24 index and water inputs to the gridbox. Within the model parameterization, the  
 25 height of the surface water level is calculated by a hypsometric function and the  
 26 gridbox fraction is further derived from the grid size. This allows an ever-  
 27 existing surface inundated fraction even in very dry gridboxes, whereas the  
 28 GIEMS method underestimates the small wetlands comprising less than 10% of  
 29 the gridbox area (Prigent et al., 2007); hence a model overestimation of satellite



1 dataset is expected. Definition of modelled and satellite derived inundated  
2 fraction is not the same. Unfortunately there is no standard definition  
3 (Reichhardt, 1995), which produces the struggle to find a proper observational  
4 dataset to evaluate model results. What we emphasize from our findings is,  
5 nevertheless, the spatial patterns of higher inundated fractions occurring at  
6 similar locations in model and satellite dataset (Fig. 6).  
7

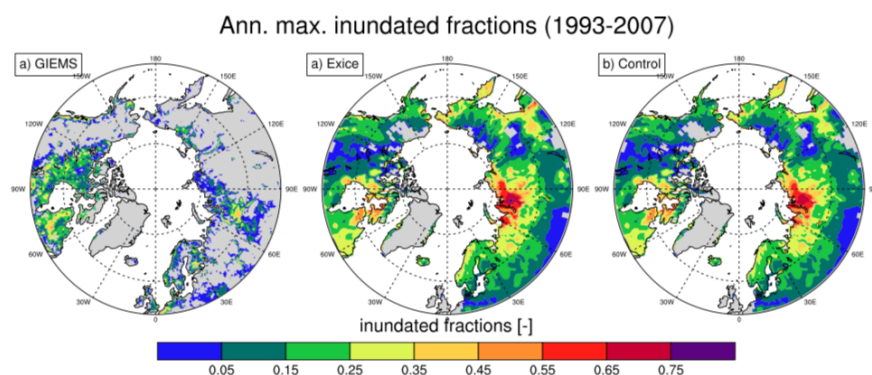


Fig. 6: Surface water fraction comparison from high latitude ( $>50^{\circ}\text{N}$ ) maps of annual maximum surface wetlands from GIEMS dataset (Prigent et al., 2012) and annual maximum  $f_{h2osfc}$  values of Exice and Control experiments for the period 1993-2007.

#### 4. Conclusion

A warming climate affects the Arctic more severely than the rest of the globe. Increasing surface temperatures pose an important threat to the vulnerable high latitude ecosystems. Degradation of Arctic permafrost due to increased soil temperatures leads to the release of permafrost carbon to the atmosphere and further strengthens the greenhouse warming (IPCC, 2013; Schuur et al., 2008). For future climate predictions, it is necessary to properly simulate the Arctic surface inundated areas due to their physical and biogeochemical coupling with the atmosphere.

This study summarizes a new parameterization within the CLM to represent prognostic surface inundated fractions under permafrost thawing using a conceptual approach that can lead to implementation of a physical process-based parameterization. Coupling ground subsidence to surface microtopography distribution, hence allowing a natural link between surface hydrological conditions and soil thermodynamics, resulted in generally increased surface inundated fractions over the northern high latitudes, with larger surface inundated fractions around western and far-east Siberian plains and northeastern Canada. Projected increase in global temperatures will inevitably cause more excess ice melting and subsequent ground subsidence, therefore, it will be necessary to incorporate a process-based parameterization to accurately account for future ground subsidence effects on surface hydrological states.

Our results confirm the enhancements of coupling ground subsidence and surface inundation to represent the temporal changes in surface hydrology



1 reflected by soil physical states and the atmospheric forcing, which is much  
2 needed for a future scenario experiment. Here we conclude that our new  
3 parameterization is implemented successfully and can be used for future climate  
4 scenarios such as shown in Lee et al. (2014) with major subsidence events  
5 during the 21<sup>st</sup> century under a high warming scenario.

6  
7 This new parameterization represents the first step into a process-based  
8 representation of such hydrological processes in CLM. Using this  
9 parameterization, further work can proceed to investigate the biogeochemical  
10 feedbacks of permafrost greenhouse gas fluxes between land and atmosphere.

11

### 12 **Code and data availability**

13 The code modifications to CLM model in accordance to this paper are accessible  
14 through the Zenodo archive with the following link:

15 <https://zenodo.org/badge/latestdoi/183611414>

16 The overall CLM model code can be obtained from the NCAR archives, the  
17 instructions on accessing the model code is given through this website:

18 <http://www.cesm.ucar.edu/models/cesm2/land/>

19 The full set of model data will be made publicly available through the Norwegian  
20 Research Data Archive at <https://archive.norstore.no> upon publication.

21

### 22 **Author contribution**

23 AE and HL designed the experiments and AE carried them out. DML and SCS  
24 developed the main CLM model code and HL developed the previous version this  
25 model is based on. CP has provided the GIEMS dataset. AE performed the  
26 simulations and prepared the manuscript with contributions from all co-authors.

27

### 28 **Acknowledgements**

29 This work was supported by the Research Council of Norway projects  
30 PERMANOR (255331) and MOCABORS (255061) and NSF EaSM-L02170157. The  
31 simulations were performed on resources provided by UNINETT Sigma2-the  
32 National Infrastructure for High Performance Computing and Data Storage in  
33 Norway, accounts NS2345K and NN2345K.

34

35

36

37

38

39

40

41

42

43

44

45

46

47

48

49



1  
2

3  
4  
5

6  
7  
8

## 10 **References**

- 11 Beven, K. and Kirkby, M.: A physically based, variable contributing area model of basin  
12 hydrology, *Hydrol. Sci. Bull. Sci. Hydrol.*, 24, 43–69, 1979.
- 13
- 14 Brown J, Ferrians, O. J. Jr., Heginbottom, J. A., and Melnikov, E. S.: Circum-Arctic Map  
15 of Permafrost and Ground-Ice Conditions version 2 (Boulder, CO: National Snow and Ice  
16 Data Center), 1997.
- 17
- 18 Chadburn, S., Burke, E., Essery, R., Boike, J., Langer, M., Heikenfeld, M., Cox, P., and  
19 Friedlingstein, P.: An improved representation of physical permafrost dynamics in the  
20 JULES land-surface model, *Geosci. Model Dev.*, 8, 1493-1508,  
21 <https://doi.org/10.5194/gmd-8-1493-2015>, 2015.
- 22
- 23 Ekici, A., Beer, C., Hagemann, S., Boike, J., Langer, M., and Hauck, C.: Simulating high-  
24 latitude permafrost regions by the JSBACH terrestrial ecosystem model, *Geosci. Model  
25 Dev.*, 7, 631–647, doi:10.5194/gmd-7-631-2014, 2014.
- 26
- 27 Gouttevin, I., Krinner, G., Ciais, P., Polcher, J., and Legout, C.: Multi-scale validation of a  
28 new soil freezing scheme for a land- surface model with physically-based hydrology, *The  
29 Cryosphere*, 6, 407–430, doi:10.5194/tc-6-407-2012, 2012
- 30



- 1 Grosse, G., Jones, B., Arp, C.: Thermokarst Lakes, Drainage, and Drained Basins,  
2 Elsevier: Amsterdam, The Netherlands, 2013.  
3  
4 IPCC: Climate Change 2013: The Physical Science Basis. Contribution of Working Group  
5 I to the Fifth Assessment Report of the Intergovernmental Panel on Climate Change  
6 [Stocker, T.F., D. Qin, G.-K. Plattner, M. Tignor, S.K. Allen, J. Boschung, A. Nauels, Y.  
7 Xia, V. Bex and P.M. Midgley (eds.)], Cambridge University Press, Cambridge, United  
8 Kingdom and New York, NY, USA, 1535 pp, doi:10.1017/CBO9781107415324, 2013.  
9  
10 Lawrence, D. M., Slater, A. G., Romanovsky, V. E., and Nicolsky, D. J.: Sensitivity of a  
11 model projection of near-surface permafrost degradation to soil column depth and  
12 representation of soil organic matter, *J. Geophys. Res.*, 113, 1–14, 2008.  
13  
14 Lawrence, D. M., Oleson, K. W., Flanner, M. G., Thornton, P. E., Swenson, S. C.,  
15 Lawrence, P. J., Zeng, X., Yang, Z. L., Levis, S., Sakaguchi, K., and Bonan, G. B.:  
16 Parameterization improvements and functional and structural advances in version 4 of  
17 the Community Land Model, *Journal of Advances in Modeling Earth Systems*, 3(1), 2011.  
18  
19 Lawrence, D.M. R.A., Fisher, C.D. Koven, K.W. Oleson, S.C. Swenson, G. Bonan, N.  
20 Collier, B. Ghimire, L. van Kampenhout, D. Kennedy, E. Kluzek, P.J. Lawrence, F. Li, H.  
21 Li, D. Lombardozzi, W.J. Riley, W.J. Sacks, M. Shi, M. Vertenstein, W.R. Wieder, C. Xu,  
22 A.A. Ali, A.M. Badger, G. Bisht, M.A. Brunke, S.P. Burns, J. Buzan, M. Clark, A. Craig,  
23 K. Dahlin, B. Drewniak, J.B. Fisher, M. Flanner, A.M. Fox, P. Gentine, F. Hoffman, G.  
24 Keppel-Aleks, R., Knox, S. Kumar, J. Lenaerts, L.R. Leung, W.H. Lipscomb, Y. Lu, A.,  
25 Pandey, J.D. Pelletier, J. Perket, J.T. Randerson, D.M. Ricciuto, B.M., Sanderson, A.  
26 Slater, Z.M. Subin, J. Tang, R.Q. Thomas, M. Val Martin, and X. Zeng: The Community  
27 Land Model version 5: Description of new features, benchmarking, and impact of forcing  
28 uncertainty. *Submitted to J. Adv. Model. Earth Syst.*, 2018.  
29  
30 Lee, H., Swenson, S. C., Slater, A. G., and Lawrence, D. M.: Effects of excess ground ice  
31 on projections of permafrost in a warming climate, *Environmental Research*  
32 *Letters*, 9(12), p.124006, 2014.  
33  
34 Liljedahl, A. K., Boike, J., Daanen, R. P., Fedorov, A. N., Frost, G. V., Grosse, G.,  
35 Hinzman, L. D., Iijima, Y., Jorgenson, J. C., Matveyeva, N., and Necsoiu, M.: Pan-Arctic  
36 ice-wedge degradation in warming permafrost and its influence on tundra  
37 hydrology, *Nature Geoscience*, 9(4), pp.312-318, 2016.  
38  
39 Melton, J. R., Wania, R., Hodson, E. L., Poulter, B., Ringeval, B., Spahni, R., Bohn, T.,  
40 Avis, C. A., Beerling, D. J., Chen, G., Eliseev, A. V., Denisov, S. N., Hopcroft, P. O.,  
41 Lettenmaier, D. P., Riley, W. J., Singarayer, J. S., Subin, Z. M., Tian, H., Zürcher, S.,  
42 Brovkin, V., van Bodegom, P. M., Kleinen, T., Yu, Z. C., and Kaplan, J. O.: Present state  
43 of global wetland extent and wetland methane modelling: conclusions from a model inter-  
44 comparison project (WETCHIMP), *Biogeosciences*, 10, 753-788,  
45 <https://doi.org/10.5194/bg-10-753-2013>, 2013.  
46  
47 Muster, S., Roth, K., Langer, M., Lange, S., Aleina, F.C., Bartsch, A., Morgenstern, A.,  
48 Grosse, G., Jones, B., Sannel, A. B. K., and Sjöberg, Y.: PeRL: A Circum-Arctic  
49 Permafrost Region Pond and Lake Database, *Earth Syst. Sci. Data*, 9, 317–348, 2017.  
50  
51 Oleson, K. W., Lawrence, D. M., Bonan, G. B., Drewniak, B., Huang, M., Koven, C. D.,  
52 Levis, S., Li, F., Riley, W. J., Subin, Z. M., Swenson, S. C., Thornton, P. E., Bozbiyik, A.,  
53 Fisher, R., Kluzek, E., Lamarque, J. -F., Lawrence, P. J., Leung, L. R., Lipscomb, W.,  
54 Muszala, S., Ricciuto, D. M., Sacks, W., Sun, Y., Tang, J., and Yang, Z. -L: Technical  
55 Description of version 4.5 of the Community Land Model (CLM), Ncar Technical Note  
56 NCAR/TN-503+STR, National Center for Atmospheric Research, Boulder, CO, 422 pp,  
57 DOI: 10.5065/D6RR1W7M, 2013.





- 1  
2 Prigent, C., Papa, F., Aires, F., Rossow, W. B., and Matthews, E.: Global inundation  
3 dynamics inferred from multiple satellite observations, 1993–2000, *Journal of*  
4 *Geophysical Research: Atmospheres*, 112(D12), 2007.
- 5  
6 Prigent, C., Papa, F., Aires, F., Jimenez, C., Rossow, W. B., and Matthews, E.: Changes  
7 in land surface water dynamics since the 1990s and relation to population  
8 pressure, *Geophysical Research Letters*, 39(8), 2012.
- 9  
10 Reichhardt, T.: Academy under fire on “wetlands” definition, *Nature*, 375, 171, 1995.
- 11  
12 Riley, W. J., Subin, Z. M., Lawrence, D. M., Swenson, S. C., Torn, M. S., Meng, L.,  
13 Mahowald, N. M., and Hess, P.: Barriers to predicting changes in global terrestrial  
14 methane fluxes: analyses using CLM4Me, a methane biogeochemistry model integrated  
15 in CESM, *Biogeosciences*, 8, 1925-1953, <https://doi.org/10.5194/bg-8-1925-2011>, 2011.
- 16  
17 Saunois, M., Bousquet, P., Poulter, B., Peregón, A., Ciais, P., Canadell, J. G.,  
18 Dlugokencky, E. J., Etiope, G., Bastviken, D., Houweling, S. and Janssens-Maenhout,  
19 G.: The global methane budget 2000-2012, *Earth System Science Data*, 8(2), p.697,  
20 2016.
- 21  
22 Schuur, E. A., Bockheim, J., Canadell, J. G., Euskirchen, E., Field, C. B., Goryachkin, S.  
23 V., Hagemann, S., Kuhry, P., Lafleur, P.M., Lee, H., and Mazhitova, G.: Vulnerability of  
24 permafrost carbon to climate change: Implications for the global carbon cycle, *AIBS*  
25 *Bulletin*, 58(8), pp.701-714, 2008.
- 26  
27 Serreze, M. C. and Francis, J. A.: The Arctic amplification debate, *Clim. Change* 76, 241–  
28 264 (2006), 2006.
- 29  
30 Solomon, S., Qin, D., Manning, M., Averyt, K., and Marquis, M. eds.: Climate change  
31 2007-the physical science basis: Working group I contribution to the fourth assessment  
32 report of the IPCC (Vol. 4), Cambridge university press, 2007.
- 33  
34 Swenson, S. C., Lawrence, D. M. and Lee, H.: Improved simulation of the terrestrial  
35 hydrological cycle in permafrost regions by the Community Land Model, *Journal of*  
36 *Advances in Modeling Earth Systems*, 4(3), 2012.
- 37  
38 Tarnocai, C., Swanson, D., Kimble, J., and Broll, J.: Northern Circumpolar Soil Carbon  
39 Database, Tech. Rep. Version 1, Research Branch, Agriculture and Agri-Food Canada,,  
40 available at: <http://wms1.agr.gc.ca/NortherCircumpolar/northercircumpolar.zip> (last  
41 access: 1 October 2012), 2007.
- 42  
43 Tarnocai, C., Canadell, J. G., Schuur, E. A. G., Kuhry, P., Mazhitova, G., and Zimov, S.:  
44 Soil organic carbon pools in the northern circumpolar permafrost region, *Global*  
45 *Biogeochem. Cy.*, 23, GB2023, doi:10.1029/2008GB003327, 2009.
- 46  
47 Treat, C.C., Natali, S.M., Ernakovich, J., Iversen, C.M., Lupascu, M., McGuire, A.D.,  
48 Norby, R.J., Roy Chowdhury, T., Richter, A., Šantrůčková, H., and Schädel, C.: A  
49 pan-Arctic synthesis of CH<sub>4</sub> and CO<sub>2</sub> production from anoxic soil incubations, *Global*  
50 *change biology*, 21(7), pp.2787-2803, 2015.
- 51  
52 Viovy, N. CRUNCEP data set.  
53 [ftp://nacp.ornl.gov/synthesis/2009/frescati/temp/land\\_use\\_change/original/readme.htm](ftp://nacp.ornl.gov/synthesis/2009/frescati/temp/land_use_change/original/readme.htm),  
54 last access: 11.12.2017.
- 55  
56 Wania, R., Melton, J. R., Hodson, E. L., Poulter, B., Ringeval, B., Spahni, R., Bohn, T.,  
57 Avis, C. A., Chen, G., Eliseev, A. V., Hopcroft, P. O., Riley, W. J., Subin, Z. M., Tian, H.,



- 1 van Bodegom, P. M., Kleinen, T., Yu, Z. C., Singarayer, J. S., Zürcher, S., Lettenmaier,  
2 D. P., Beerling, D. J., Denisov, S. N., Prigent, C., Papa, F., and Kaplan, J. O.: Present  
3 state of global wetland extent and wetland methane modelling: methodology of a model  
4 inter-comparison project (WETCHIMP), *Geosci. Model Dev.*, 6, 617-641,  
5 <https://doi.org/10.5194/gmd-6-617-2013>, 2013.  
6  
7 Zona, D., Lipson, D. A., Zulueta, R. C., Oberbauer, S.F., and Oechel, W. C.:  
8 Microtopographic controls on ecosystem functioning in the Arctic Coastal Plain, *Journal*  
9 *of Geophysical Research: Biogeosciences*, 116(G4), 2011.  
10